

Elastic scattering of negative pions from ^{16}O and Ca in the 3,3 resonance region

M. Blecher, K. Gotow, and D. K. Anderson

Virginia Polytechnic Institute and State University, Blacksburg, Virginia 24061*

R. Kerns,[†] R. Minehart, and K. Ziock

University of Virginia,[‡] Charlottesville, Virginia 22901

R. W. Bercaw and J. S. Vincent[§]

National Aeronautics and Space Administration, Lewis Research Center, Cleveland, Ohio 44135

R. Johnson

University of British Columbia, Vancouver 8, British Columbia, Canada

(Received 3 July 1974)

The elastic scattering cross sections for $\pi^-^{16}\text{O}$ and π^- -Ca have been measured at pion kinetic energies 160, 170, 220, 230, and 240 MeV for ^{16}O , and at 205 and 215 MeV for Ca. The results are analyzed in terms of the Kisslinger and Laplacian optical model potentials and the obtained potential parameters are compared with the impulse approximation result.

NUCLEAR REACTIONS Ca(π , π), O(π , π), $E = 160$ – 240 MeV; measured $\sigma(E, \theta)$; deduced optical-model parameters. Natural target, resolution 3 MeV; $\theta = 15$ – 70° , $\Delta\theta = 2^\circ$.

I. INTRODUCTION

Pion-nucleus scattering at energies near 190 MeV has been drawing increasing attention. The fact that the elementary process π -nucleon interaction, has a broad resonance in the production of a nucleon isobar ($J = \frac{3}{2}$, $I = \frac{3}{2}$) at this energy, and that consequently the p -wave π -nucleon interaction dominates the elementary scattering process, gives a unique situation in nuclear physics. For example, an optical model potential description of the π -nucleus elastic scattering must reflect the presence of the π -nucleon resonance and is expected to be quite different in physical content from optical potentials for other processes such as proton-nucleus elastic scattering. Besides, the effects of pion absorption in nuclear matter must be incorporated in the inelastic contributions of the optical model potential.

In the past several years considerable experimental work on this subject has been done for limited kinds of target nuclei. Notable among this work are the experiments of Binon *et al.*¹ and of Rohlin *et al.*² The main portion of the existing data, consisting of elastic scattering of π^- from ^{12}C , has been analyzed in terms of optical potentials by Krell and Bramo³ and by Sternheim and Auerbach.⁴

Theoretical work on pion-nucleus scattering can be summarized in general by stating that various models have been developed using optical poten-

tials,⁵ the concept of the index of refraction in nuclear matter,⁶ the Glauber approximation,⁷ and multiple-scattering series.⁸

Agreements between the data and theoretical results on pion-nuclear scattering around the resonance energy are, in general, good only in a qualitative sense and some detailed studies³ on energy dependence of the goodness of fit show that the low energy optical model potential³ must be modified at the resonance energy in order to give a truly quantitative description of the process.

The motivations of the work presented here are to add substantial amounts of data to the existing ones using typical light and medium heavy nuclei, to compare our result with the ^{12}C scattering data in order to test whether the conclusions thus far obtained are valid for other nuclei, and also to learn whether pion elastic scattering can be used to determine the values of the parameters in a given optical model potential.

This article describes details of measurements on π^- elastic scattering differential cross sections from ^{16}O and natural Ca in the energy range of 160 to 240 MeV, along with analyses of the data obtained.

On our result of $\pi^-^{16}\text{O}$, a brief letter has already been published.⁹ Also a single energy measurement of $\pi^+^{16}\text{O}$ has been made by Rohlin *et al.*,² and their elastic scattering angular distribution has been analyzed in terms of optical model potential by Koch and Sternheim⁵ as well as with the Glauber approximation.²

II. EXPERIMENTAL PROCEDURE

The layout of the experiment is shown in Fig. 1. Two identical magnetic spectrometers were used to measure the momentum loss of the scattered particles in the following way. The trajectories of the particles were determined from the location of sparks in eight sonic spark chambers,¹⁰ four associated with each spectrometer. In order to vary the scattering angle the second spectrometer was mounted on a platform pivoted at the target position. Using measured magnetic field maps and the trajectory of a particle, its momentum before and after scattering was calculated. After plotting the number of events as a function of energy loss, elastically scattered particles were separated from the background.

Pion beams

Negative pions were produced internally in the 600 MeV Space Radiation Effects Laboratory synchrocyclotron with a carbon harp target and deflected out of the cyclotron by the fringing field of the cyclotron magnet. The quadrupole doublet, Q1-Q2, focused the beam onto a uranium slit, S1, in the main shielding wall. The bending magnet M1 separated the charged particles from neutral radiation and swept away low momentum charged background particles. The quadrupole doublet Q3-Q4 then focused the beam onto the target. The beam was detected in counters SC1, SC2 (17.5 cm × 22.5 cm × 0.64 cm) at the beginning of the first spectrometer and by SC3 (22.5 cm × 17.5 cm × 0.16 cm) located at the target. For the purpose of the experiment the incident beam was then defined by a triple coincidence (SC1, SC2, SC3). No efficiency correction was needed for this coincidence as any particles not counted made no contribution to the experiment.

By adjusting the location of magnets Q1, Q2, and M1 we could select a range of energies from 160 to 250 MeV.

Targets

The target was located at the pivot point of the second spectrometer and was oriented for transmission geometry. The various targets used were of the order of 2 g/cm² thick and were 15 cm × 15 cm in cross section. For scattering on ¹⁶O, we used a water target with Mylar walls, 0.051 cm thick. Background runs were made with an identical empty target.

Scattering logic

Two identical scintillation counters SC4 and SC5, the dimensions of which were 30 cm high,

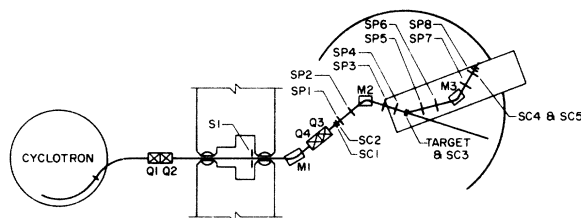


FIG. 1. Layout of the experiment: Q, quadrupole magnets; M, bending magnets; SP, sonic spark chambers; SC, scintillation counters.

45 cm wide and 0.64 cm thick, were used to detect the scattered particles. A scattering event was defined by the coincidence (SC1, SC2, SC3, SC4, SC5). In separate measurements a precise value for the ratio (SC1-5)/(SC1-3) was determined. Much longer measurements with the sonic chambers triggered by the coincidence (SC1-5) determined what proportion of the scattered events represented elastic pion-nucleus scattering.

Spectrometers

The two spectrometers were identical except that the second was mounted on a movable platform. The spectrometer consisted of a dipole magnet with a useful gap of 50 cm × 50 cm × 22.5 cm high. Four sonic spark chambers of the type described elsewhere¹⁰ were rigidly mounted to a frame fastened to the yoke of the magnet. Two chambers were used at the entrance to the magnet, and two at the exit. Since any three of these were sufficient to determine the trajectory, we accepted events in which any three of the four worked satisfactorily. High voltage to the spark chambers was supplied through a pulser triggered by the (SC1-5) coincidence.

The chambers were aligned to an accuracy of 0.1 mm relative to the pole pieces of each magnet and the magnets were placed on a nominal beam line drawn on the floor. The accuracy of spark reconstruction in the sonic chambers was approximately ± 0.5 mm. For final calibration, data were taken without a target and with a scattering angle of 0°. In this case the spark chambers were triggered on particles passing directly through all eight. Any relative misalignment of the two spectrometers could be determined from the requirements that the momentum obtained from each be the same, and that the trajectory through SP3, SP4, SP5, and SP6 should be a straight line, except for multiple scattering.

To reduce the effects of multiple scattering in the spectrometers, helium filled bags were used between each pair of chambers. The spark cham-

bers SP2, SP3, SP6, and SP7 also were constructed with thinner aluminum foils (0.008 mm) than were the other four (0.025 mm).

In analyzing the data for each event, the scattering angle was determined from spark chambers SP3 through SP6. Momenta were calculated for each spectrometer and from this the energy loss was obtained. Thus each event is classified by its scattering angle, its incident momentum, and its energy loss.

Magnetic field maps

The bending magnets M2 and M3 used in the spectrometers were constructed identically. Their fields were mapped on a grid of 3000 points and stored on magnetic tape, using an automatic mapping device. For on-line computer analysis the effective lengths of the magnets as a function of the point of entry into the field were calculated. For off-line computer analysis, initially a ray tracing program¹¹ obtained from CERN was used to fit the spark coordinates to a momentum by numerical ray tracing through the grid of field points. Later a set of Tschebycheff polynomials were constructed following the method of Lechanoine, *et al.*¹² to represent the momentum as a function of the spark coordinates. With the second method the computer time required to obtain the momentum for a trajectory was reduced by a factor of 1000.

Electronic circuitry

The logic of the experiment was straightforward and the electronic circuitry required was simple. A scattering pion was defined as a coincidence between scintillation counters 1 through 5. Counters 1, 2, and 3 defined the incident beam on the target, while counters 4 and 5 defined a scattered pion. When such a coincidence occurred, an electrical signal was generated that was used to trigger the high voltage to the spark chambers, using spark gap triggers manufactured by Science Accessories Corporation. After a delay of 20 μsec a 2 MHz clock was started and its pulse train was fed into a bank of scalers, one scaler for each sonic chamber microphone. Receipt of a signal from the microphone shut off the corresponding scaler. After waiting 5 msec for digitization of the microphone outputs, the event was read into the computer.

Since four of the spark chambers were operating in the incident beam, it was necessary to operate the chambers with as short a sensitive time as possible. The clearing field was adjusted for minimum sensitive time, ~ 500 nsec. To minimize the delay between the passage of a particle and the ap-

plication of high voltage to the spark chambers, the electronic circuits used in the trigger logic were located inside the experimental cave. A duplicate set of circuits was used outside the cave.

In addition to the event logic the electronic circuitry provided a number of gates. A "RF gate" shut off the logic circuitry during the "prompt" portion of the beam spill to avoid triggering the chambers when the instantaneous intensity was very high. A "computer busy gate" shut off the circuits during periods when the computer was unable to accept data. Following an event a 0.5 sec gate held the logic circuits off to allow time to digest the data with the on-line program. This did not affect the data-taking rate significantly at the large angles where the rate was slow enough to limit the statistical accuracy of the data.

Beam composition

The beam composition was determined in two ways. One was a direct measurement using a time-of-flight arrangement. The second method was to measure the differential cross section for ^{12}C at $\theta_{\text{lab}} = 25^\circ$, 27° , and 29° and normalize it to the data of Binon *et al.*¹ This normalization was cast in terms of the percentage of pions in the beam.

The time-of-flight measurement was carried out with two small scintillation detectors (5 cm \times 5 cm), one at the position of the slit S1 and the other at the target position. The delay time between two nearly coincident signals was converted by a time to amplitude converter to a pulse height that was stored in a multichannel analyzer. The distribution of events vs pulse height was fitted to empirical line shapes based on the resolution of the system in order to determine the pion content. Typical results are presented in Fig. 2, which also shows a computed fit. The proportion of pions in the beam could be determined to an accuracy of

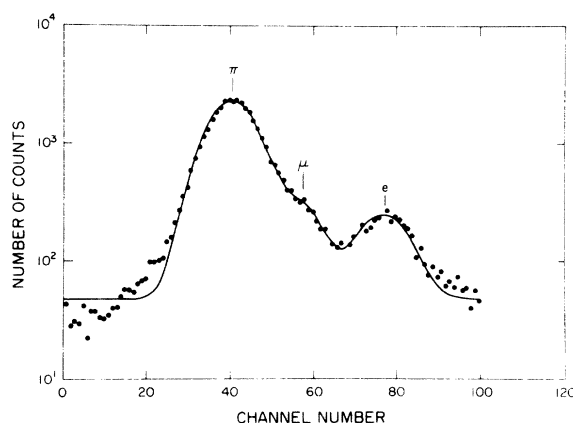


FIG. 2. Typical time of flight distribution.

~2%. Typically, the fraction was about 85%. No correction for pion decay between the two counters was made. A computer calculation indicated that the number of pions which decay but nevertheless still appear in the pion peak was negligible.

For energies above 200 MeV, the time-of-flight apparatus did not have sufficient resolution, and we relied entirely on the carbon normalization.

$\theta_s \pm \frac{1}{2}\gamma$ is calculated as

$$\frac{d\sigma}{d\Omega}(E_0, \theta_s) = \frac{N_E(\theta_0, \theta_s \pm \frac{1}{2}\gamma, E_0 \pm \frac{1}{2}\delta)}{N(\theta_0)} \frac{N_{12345}}{N_{123}} \left[n f_\pi B(E_0 \pm \frac{1}{2}\delta) \Sigma_{sc4} \Sigma_{sc5} \left(\prod_{i=1}^8 \Sigma_{spi} \right) \Delta\Omega(\theta_0, \theta_s \pm \frac{1}{2}\gamma, E_0 \pm \frac{1}{2}\delta) \mu(\theta_0, E_0) \right]^{-1},$$

where $\gamma = 2^\circ$, $\delta = 10$ MeV, n is the number of target nuclei per unit area, θ_0 is the spectrometer angle setting, and Σ_{sc_i} and Σ_{spi} are the efficiencies of the i th scintillation counter and sonic chamber, respectively.

The number of elastic events N_E was extracted from the energy loss spectrum, obtained by the sonic chamber spectrometer, containing the total number of analyzed scattering events $N(\theta_0)$. A typical energy loss spectrum is shown in Fig. 3.

The number of coincidences SC1 through SC5, N_{12345} , corresponded to the number of all types of events detected through the spectrometer for a given number of the incident particles, N_{123} .

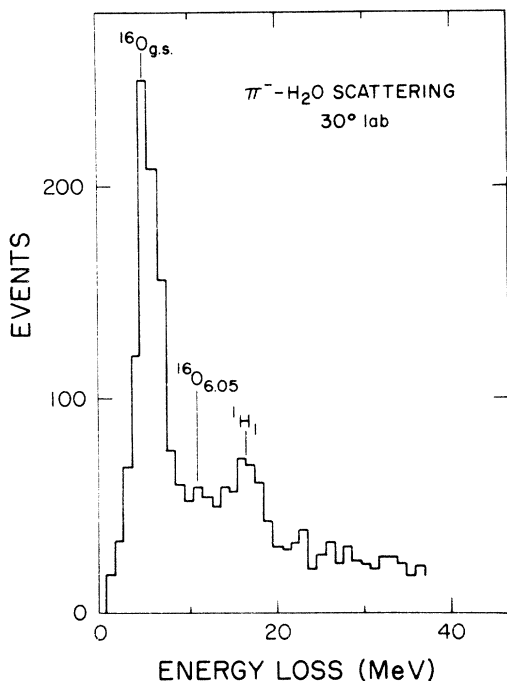


FIG. 3. Typical energy loss spectrum of pions scattered from a water target.

Where the time of flight technique was used, comparison between it and the carbon normalization gave agreement to within the experimental errors.

III. DATA ANALYSIS

The elastic scattering cross section for negative pions of energies $E_0 \pm \frac{1}{2}\delta$ with scattering angles

$B(E_0 \pm \frac{1}{2}\delta)$ is the fraction of the incident particles with the momentum corresponding to the pion energy ($E_0 \pm \frac{1}{2}\delta$). It was obtained by triggering the chambers 1 through 4 on the (SC1, SC2, SC3) coincidences and examining the resulting energy spectrum. The fraction f_π of pions in $B(E_0 \pm \frac{1}{2}\delta)$ was determined as described in Sec. II.

The solid angle $\Delta\Omega$ and decay correction factor $\mu(\theta_0, E_0)$ were calculated via Monte Carlo techniques. For the solid angle we considered the distributions of the incident pion energy and direction which were known from the sonic chamber data used to obtain $B(E_0 \pm \frac{1}{2}\delta)$. A pion in these distributions was allowed to scatter elastically at random angles—and the scattering angle bin incremented. The pion was followed through the magnetic field by the same program used to make the momentum analysis. If it passed through the spectrometer correctly the array corresponding to the number of successes for a given scattering angle bin was incremented. By repeating this procedure, the solid angle was obtained.

For the decay correction we started with pions of energies $< E_0 + \frac{1}{2}\delta$ moving in the direction defined by θ_0 . The pion was allowed to decay at random (weighted by the exponential decay factor) in its rest frame, and the point of decay and momentum and direction of the resulting muon in the laboratory were obtained. This muon was traced through the spectrometer, and if it could be detected by SC4 and SC5, its energy was calculated assuming the particle was a pion. Finally, this energy was compared with the energies accepted for elastic scattering events. In this way, for a given number of elastically or inelastically scattered pions, we found the fraction which survived as only elastically scattered events.

IV. EXPERIMENTAL RESULTS AND ANALYSIS

The observed differential cross sections for π^- - ^{16}O and π^- -Ca elastic scattering are listed on Ta-

TABLE I. Differential elastic scattering cross sections for π^- - ^{16}O in the laboratory system. The cross sections are in mb/sr and the errors are standard deviations due to counting statistics and solid angle calculations. The absolute error of $\pm 15\%$ is not included.

$T\pi=160$ MeV			$T\pi=170$ MeV			$T\pi=220$ MeV			$T\pi=230$ MeV			$T\pi=240$ MeV		
θ_{lab}	$d\sigma/d\Omega$	$\Delta(d\sigma/d\Omega)$												
13	988	117	13	667	80	15	297	46	15	383	39	15	396	44
15	667	78	15	500	60	17	317	45	17	253	33	17	268	38
17	533	63	17	388	35	19	268	81	19	270	30	19	218	65
19	380	35	19	320	26	21	219	27	21	192	19	21	214	26
21	276.3	23	21	260	21	23	138	21	23	135	16	23	125	20
23	230.5	20.8	23	179.6	13.5	25	85.4	11.8	25	93.4	8.5	25	86.0	10.6
25	168.4	13.1	25	139.3	10.7	27	65.7	9.3	27	75.2	7.9	27	58.4	9.0
27	119.9	10.0	27	116.9	8.8	29	54.3	10.0	29	47.8	5.6	29	33.0	4.1
29	84.3	6.8	29	85.4	6.1	31	35.7	3.5	31	16.8	1.7	31	12.50	2.0
31	69.1	5.4	31	49.8	4.1	33	8.78	1.73	33	6.88	1.05	33	4.18	1.26
33	57.5	5.6	33	43.2	3.5	35	6.04	1.15	35	6.42	0.96	35	4.20	1.01
35	27.3	2.6	35	24.1	2.2	37	4.82	0.97	37	2.60	0.56	37	2.43	0.67
37	17.6	2.0	37	14.4	1.4	39	2.75	0.85	39	2.17	0.31	39	2.45	0.41
39	12.4	1.3	39	7.73	0.88	41	0.928	0.348	41	1.44	0.27	41	2.48	0.43
41	8.14	0.93	41	6.23	0.79	43	2.53	0.45	43	1.90	0.29	43	2.58	0.51
43	2.17	0.36	43	1.64	0.22	45	2.63	0.65	45	2.96	0.51	45	6.38	0.88
45	1.71	0.23	45	1.31	0.18	47	3.26	0.64	47	3.32	0.54	47	5.52	0.92
47	1.98	0.25	47	0.173	0.092	49	3.03	0.53	49	4.51	0.47	49	6.14	0.70
49	0.824	0.19	49	0.415	0.126	51	5.25	0.88	51	4.27	0.58	51	4.67	0.81
51	1.19	0.21	51	1.77	0.27	53	5.87	0.93	53	4.05	0.57	53	3.07	0.73
53	1.53	0.30	53	2.48	0.30	55	1.96	0.46	55	2.81	0.37	55	3.72	0.58
55	3.50	0.39	55	2.471	0.30	57	2.24	0.44	57	2.70	0.36	57	3.36	0.54
57	3.53	0.40	57	4.48	0.46	59	1.70	0.28	59	1.44	0.19	59	1.48	0.26
59	3.70	0.40	59	2.55	0.29	61	1.75	0.33	61	1.10	0.18	61	1.07	0.18
61	2.37	0.29	63	2.48	0.26	63	1.30	0.24	63	0.523	0.133	63	0.995	0.222
63	2.63	0.34	65	1.93	0.23	69	0.438	0.163	69	0.231	0.102	69	0.152	0.078
65	2.71	0.29	67	1.03	0.18	71	0.135	0.083	71	0.160	0.063	71	0.023	0.034
67	1.63	0.21	67	1.50	0.18	76	0.162	0.115	76	0.019	0.030	76	0.057	0.085
69	2.04	0.21	69	1.42	0.16									
71	1.22	0.15	73	0.178	0.022									
73	0.293	0.038	75	0.089	0.017									
75	0.150	0.022												
77	0.157	0.022												

bles I and II. The over-all energy resolution is 3.0 to 3.5 MeV full width at half-maximum (FWHM) as determined from the width of the elastic peak in the energy loss spectra. Thus, discrimination against the contamination of inelastic scattering events is complete for the ^{16}O case but is not so for the Ca case. Calculations¹³ of inelastic scattering leading to the low lying ^{40}Ca excited states indicate that in the present angular range the amount of the total inelastic contamination is quite negligible. The errors quoted in Tables I and II are due to the counting statistics and the statistical errors of 3–4% from the Monte Carlo calculations of the solid angle. The absolute scale of the differential cross sections has an estimated error of $\pm 15\%$.

To compare our observed data with models of the pion-nuclear interaction we have calculated the elastic scattering cross sections using some potential models. The cross sections were ob-

tained by solving numerically the wave equation

$$(\vec{\nabla}^2 + k^2)\psi(\vec{r}) = 2m(V_C + V)\psi(\vec{r}). \quad (1)$$

In Eq. (1), V_C is the Coulomb potential, V the assumed pion-nucleus optical model potential, k the barycentric momentum, and $m = E_\pi E_t (E_\pi + E_t)^{-1}$ is a relativistic reduced mass defined in terms of the center-of-mass energies E_π and E_t of the pion and target nucleus, respectively.

Two rather different forms of the coordinate space optical potential have been used to study pion-nuclear interactions in the resonance region. The first form was originally introduced by Kisslinger¹⁴ to describe pion-nuclear elastic scattering at energies well below the resonance energy. However, previous work has demonstrated that the Kisslinger model interaction gives a reasonable description of elastic scattering in the resonance region as well. The Kisslinger potential is nonlo-

TABLE II. Differential elastic scattering cross sections for π^- -Ca in the laboratory system. The cross sections are in mb/sr, and the errors are standard deviations due to counting statistics and solid angle calculations. The absolute error of $\pm 15\%$ is not included.

θ_{lab}	$T\pi = 205$ MeV		$T\pi = 215$ MeV		
	$d\sigma/d\Omega$	$\Delta(d\sigma/d\Omega)$	$d\sigma/d\Omega$	$\Delta(d\sigma/d\Omega)$	
15	861	118	15	919	103
17	1222	159	17	674	78
19	610	57	21	527	50
21	507.3	67.9	23	236	29
23	559.7	55.3	25	98.9	11.1
25	190.1	58.2	27	51.4	6.4
27	82.6	9.5	29	22.5	4.4
29	29.1	5.9	31	23.6	5.3
31	36.5	4.2	33	35.8	5.0
33	51.2	6.1	35	30.3	6.8
35	43.9	4.0	37	34.7	4.1
37	59.8	6.5	39	32.6	4.4
39	56.3	6.6	41	29.5	4.1
41	44.7	4.0	43	18.5	3.0
43	43.9	5.7	45	12.6	3.9
45	26.9	2.8	47	9.89	1.55
47	21.2	2.7	49	5.66	1.55
49	13.2	1.6	51	3.88	0.84
51	5.94	0.86	53	1.75	0.57
53	4.08	0.92	55	1.81	0.57
55	3.01	0.63	57	1.52	0.50
57	4.13	0.91	59	2.00	0.49
59	5.44	1.07	61	1.96	0.36
61	3.43	0.51	63	1.16	0.26
63	3.60	0.56	65	0.660	0.145
65	1.50	0.78	67	0.601	0.155
67	0.82	0.20	69	0.242	0.097
69	1.12	0.24			
71	0.59	0.17			

cal and has the structure

$$-2mV_K(\vec{r}) = b_0 k^2 \rho(\vec{r}) - c_0 \vec{\nabla} \cdot \rho(\vec{r}) \vec{\nabla}, \quad (2)$$

where b_0 and c_0 are complex parameters and $\rho(\vec{r})$ is the nuclear matter density. The gradient terms in (2) originate from the strong momentum dependence of the pion-nucleon p -wave interaction. In the weak-binding impulse approximation the complex parameters b_0 and c_0 can be expressed in terms of the pion-nucleon s - and p -wave phase shifts, respectively.

A second form of the pion-nucleus potential is obtained with an extrapolation of the pion-nucleon scattering amplitudes into off-the-energy shell as discussed in detail by Fäldt.⁵ In this treatment the effective potential is local, but involves a Laplacian operator acting on the nuclear density. The Laplacian potential has the form

$$-2mV_L(\vec{r}) = (b_0 + c_0) k^2 \rho(\vec{r}) + \frac{1}{2} c_0 \nabla^2 \rho(\vec{r}), \quad (3)$$

where in the weak-binding impulse approximation

the complex parameters b_0 and c_0 are the same parameters that appear in Eq. (2). The Laplacian or local potential has also been used to describe elastic scattering in the resonance region and both potentials give results in agreement with existing experimental data.

To calculate the cross sections in the weak-binding impulse approximation, we have used both the Kisslinger and Laplacian potentials with the Fermi averaged parameters of Ref. 4 to fix the potential strengths b_0 and c_0 . These numerical values are given in Table III. To represent the nuclear matter density of Ca we used a Fermi three-parameter distribution

$$\rho(r) = \rho_0 \left[1 + w \left(\frac{r}{c} \right)^2 \right] \left[1 + \exp \left(\frac{r-c}{a} \right) \right]^{-1} \quad (4)$$

normalized to the number of nucleons, where $c = 3.67$ fm, $a = 0.58$ fm and $w = -0.08$ as determined from electron scattering.¹⁵ The calculated results for Ca involving no free parameters are compared with the experimental cross sections in Fig. 4. We note that both potential models give similar predictions except at large angles. In particular, both models predict two diffraction minima, but the predicted minima are much deeper than those observed. There also exists a sizable discrepancy in the magnitude of the cross section and the calculated values do not have the energy dependence of the data.

Similar calculations made for the ^{16}O data, using the Kisslinger potential and the Fermi-averaged⁴ b_0 and c_0 , are shown on Fig. 5. The parametrization of the nuclear shape is

$$\rho(r) = \rho_0 \left[1 + w \left(\frac{r}{a} \right)^2 \right] \exp \left(-\frac{r^2}{a^2} \right)$$

$w = 1.6$, $a = 1.74$ fm for the charge distribution, and 1.67 fm for the nucleon distribution. The cross sections at forward angles and the positions of the minimum and the maximum agree well with the calculated values, but the calculations do not reproduce the depth and the height of the structure around the minimum. The discrepancy at 240 MeV between the data and our calculation is very similar to that for π^- - ^{16}O at 270 MeV as seen by Koch and Sternheim of Ref. 5. In general, however, the agreement of the data with the calculated results involving no free parameters is better for ^{16}O than for Ca.

Best-fit potential parameters

The potential parameters for Ca were obtained with a least-squares fit to the data using both the Kisslinger and Laplacian potentials. The cross section with the best-fit parameters for Ca is shown on Fig. 4. The two different potentials give

TABLE III. Parameters used in the optical model calculations. The Fermi-averaged parameters (F) are the same for both the Kisslinger (K) and Laplacian (L) potential models. The best-fit parameters are given together with their estimated uncertainties.

T (MeV)		$\text{Re}(b_0)$ (fm^3)	$\text{Im}(b_0)$ (fm^3)	$\text{Re}(c_0)$ (fm^3)	$\text{Im}(c_0)$ (fm^3)
π^- -Ca					
205	F	-0.54	0.33	-0.83	6.40
	K	-1.91 ± 2.14	-1.76 ± 1.83	-3.40 ± 3.44	7.75 ± 2.63
	L	4.4 ± 2.8	-8.4 ± 8.8	-9.2 ± 3.0	11.1 ± 8.6
215	F	-0.49	0.33	-1.41	5.53
	K	0.03 ± 1.77	-0.65 ± 1.33	-4.63 ± 2.47	5.41 ± 1.82
	L	3.75 ± 2.57	-4.88 ± 4.04	-7.60 ± 2.46	7.34 ± 4.21
π^- - ^{16}O					
160	F	-0.69	0.37	2.7	8.0
	K	-0.04 ± 2.4	-2.9 ± 2.0	0.5 ± 4.6	17 ± 3
170	F	-0.65	0.36	1.6	7.7
	K	-0.70 ± 1.6	-2.0 ± 1.0	2.2 ± 2.9	13 ± 1
220	F	-0.48	0.32	-1.6	5.3
	K	5.80 ± 2.5	2.1 ± 0.9	-5.3 ± 1.6	5.3 ± 1.0
230	F	-0.44	0.32	-2.0	4.7
	K	3.20 ± 1.4	1.4 ± 0.9	-3.2 ± 1.1	5.9 ± 0.9
240	F	-0.41	0.32	-2.1	4.2
	K	1.50 ± 2.3	2.8 ± 1.4	-1.1 ± 1.8	5.1 ± 1.4

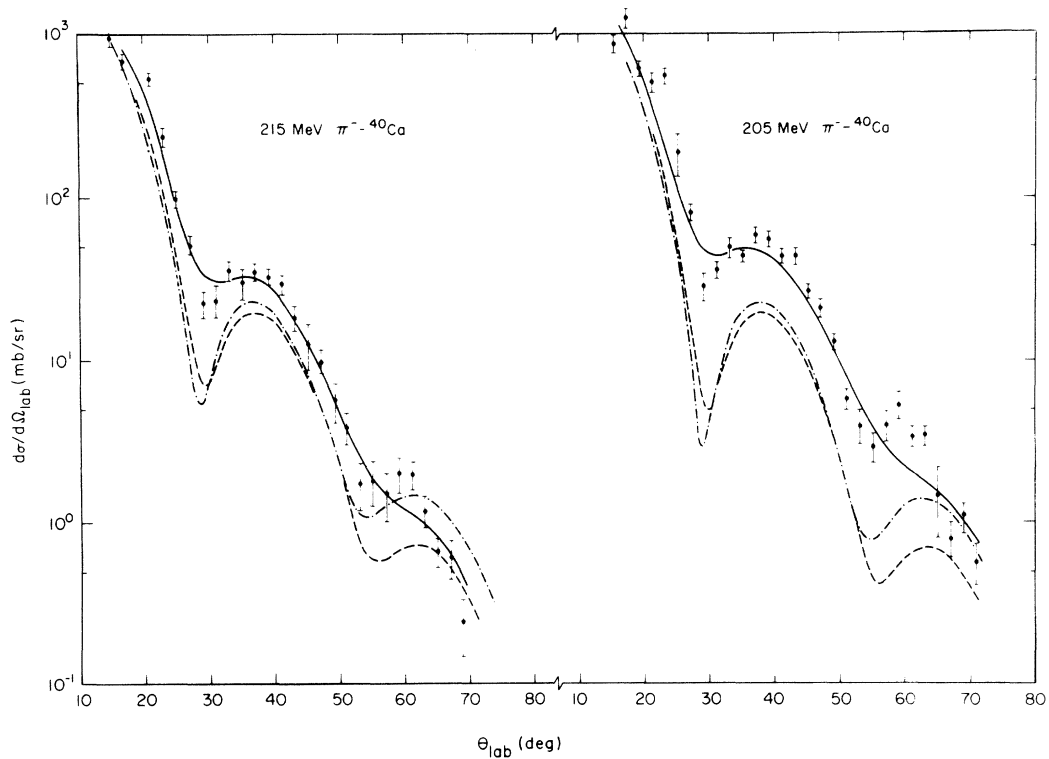


FIG. 4. Experimental differential cross section for π^- -Ca; —, best fit curve to the experimental data; ---, the cross section calculated from the Laplacian potential with the Fermi-averaged parameters; -.-, the cross section calculated from the Kisslinger potential with the Fermi-averaged parameters.

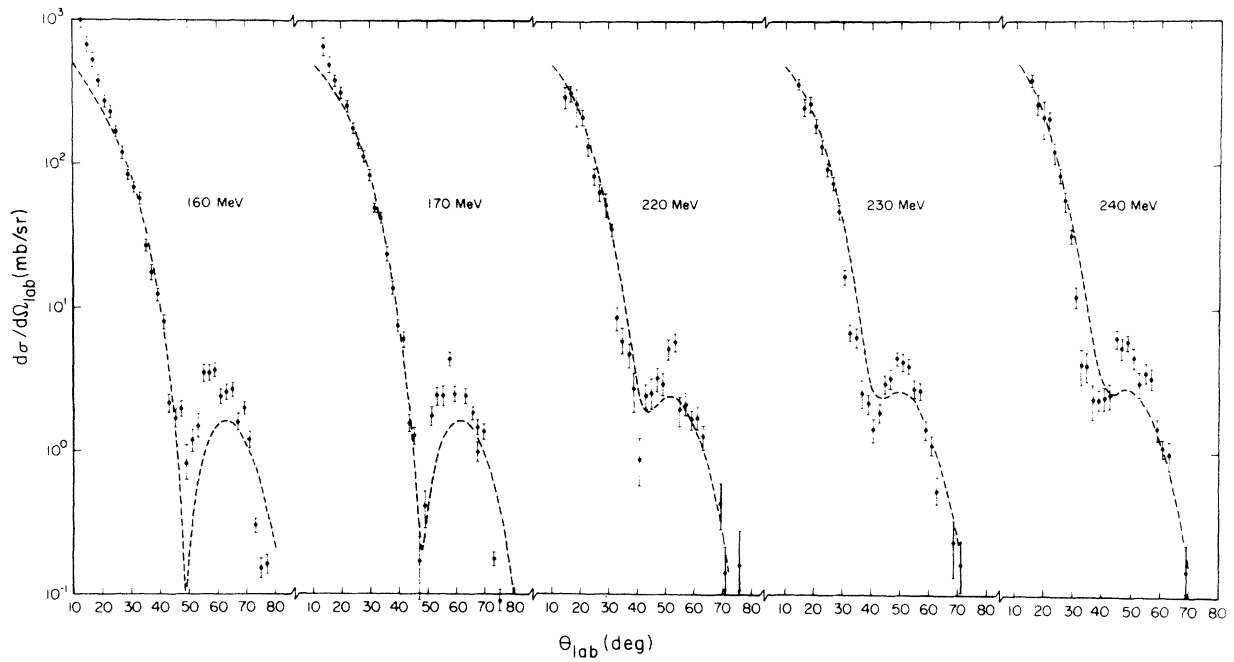


FIG. 5. Experimental differential cross section for π^- - ^{16}O ; ----, the cross section calculated from the Kisslinger potential with the Fermi-averaged parameters.

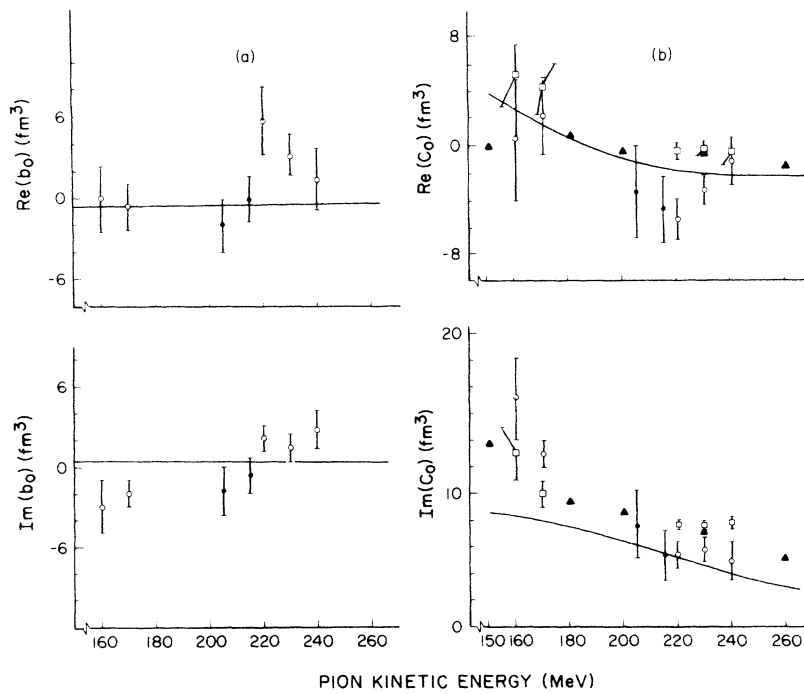


FIG. 6. Kisslinger potential parameters vs pion laboratory kinetic energy: \circ , present work on ^{16}O ; \bullet , present work on Ca; \blacktriangle , Ref. 4 on ^{12}C ; \square , same as \circ , but the best fit c_0 with b_0 set at zero.

nearly identical curves and the best-fit parameters for both models agree within the rather large error limits as listed in Table III. Similar fitting, using the Kisslinger potential, has been made for ^{16}O , the result of which was already reported in Ref. 9. The best-fit parameters for ^{16}O are also included in Table III.

The best fit optical potential parameters of the Kisslinger type potential for ^{16}O and Ca as functions of the pion laboratory kinetic energy are plotted in Fig. 6. The solid lines on the figures are the Fermi-averaged parameters obtained from the π -nucleon amplitudes. The ^{12}C parameters of Ref. 4 are also shown for comparison and were obtained for the best fit with the b_0 values fixed at appropriate Fermi-averaged values. The $\text{Re}(b_0)$ and $\text{Im}(b_0)$ for both ^{16}O and Ca are very poorly determined and at some energies $\text{Im}(b_0)$ is negative. For $\text{Re}(c_0)$ qualitative agreement exists between the Fermi-averaged and the experimentally determined values. The consistency among the potential parameters, particularly those of ^{12}C and ^{16}O , may be seen by comparing the c_0 for ^{12}C of Ref. 4 with our values of the c_0 for ^{16}O with b_0 set to zero.

The same consistency exists for $\text{Im}(c_0)$. Here, however, we can see that the energy dependence

is similar to that of the Fermi averaged parameter, but the experimental values are consistently higher than the Fermi-averaged values. This feature was first pointed out by Fäldt⁵ for the ^{12}C data, but we observe it to be the same for ^{16}O , thus supporting the view point of Fäldt that in the standard Kisslinger model b_0 is enhanced by a factor which is the squared ratio of the laboratory to the center of mass momenta of pions.

The present experimental results, however, are not precise enough to make a direct comparison of the Kisslinger and Laplacian potentials.

ACKNOWLEDGMENTS

The authors are grateful to the Space Radiation Effects Laboratory for their excellent support during this work. They also thank Professor E. S. Rost for providing us with his calculation on the π^- -Ca inelastic scattering cross section, Dr. R. H. Landau for valuable discussions, and Professor I. Tabakin for communicating to us his calculations on ^{16}O and ^{40}Ca prior to publication. The effort of Professor E. T. Boschitz in the initial stage of this experiment was instrumental in completion of the work reported.

*Work supported in part by the National Aeronautics and Space Administration under Grant Nos. NGL 47-003-044 and NASA 3 14873 and by the National Science Foundation under Grant No. GP-34618.

†Present address: Business School, East Carolina University, Greenville, North Carolina 21834.

‡Work supported in part by the National Aeronautics and Space Administration under Grant No. NGR 47-005-067, Research Corporation under Grant No. 5335/307, and the U. S. Atomic Energy Commission under Contract No. AT-(40-1)-4043.

§Present address: University of Victoria and TRIUMF, Victoria, British Columbia, Canada.

¹F. Binon, P. Duteil, J. P. Garron, J. Gorres, L. Hugun, J. P. Peignex, C. Schmit, M. Spighel, and J. P. Stroot, Nucl. Phys. **B17**, 168 (1970).

²J. Rohlin, S. Rohlin, B. W. Allardyce, J. J. Domingo, C. H. Q. Ingram, N. W. Tanner, E. M. Rimmer, and J. P. Girardeau-Montaut, Nucl. Phys. **B37**, 461 (1972).

³M. Krell and S. Barmo, Nucl. Phys. **B20**, 461 (1970).

⁴M. Sternheim and E. Auerbach, Phys. Rev. Lett. **25**, 1500 (1970).

⁵L. S. Kisslinger and W. L. Wang, Phys. Rev. Lett. **30**, 1071 (1973); J. P. Dedonder, Nucl. Phys. **A174**, 251 (1971); **A170**, 474 (1972); H. K. Lee and H. McManus, *ibid.* **A167**, 257 (1971); G. Fäldt, Phys. Rev. C **5**, 400 (1972); D. P. Engelberg, *ibid.* **6**, 1620 (1972); R. H. Landau, S. C. Phatak, and F. Tabakin, *ibid.* **7**, 1803 (1973); M. Dillig and M. G. Huber, Phys. Lett. **48B**, 417 (1974); J. H. Koch and M. M. Sternheim, Phys. Rev. C **6**, 1118 (1972).

⁶T. E. O. Ericson and J. Hüfner, Phys. Lett. **33B**, 601 (1970); C. B. Dover, J. Hüfner, and R. H. Lemmer, Ann. Phys. (N.Y.) **66**, 248 (1971); C. B. Dover and R. H. Lemmer, Nuovo Cimento Lett. **4**, 487 (1972); H. A. Bethe, Phys. Rev. Lett. **30**, 105 (1973).

⁷C. Schmit, Nuovo Cimento Lett. **4**, 454 (1970); C. Wilkin, Nuovo Cimento Lett. **4**, 491 (1970); H. Bjornenkak *et al.*, Nucl. Phys. **B22**, 179 (1970); J. P. Mallet, C. Schmit, and J. P. Dedonder, Nuovo Cimento Lett. **1**, 191 (1971); M. P. Locher, O. Steinman, and N. Strauman, Nucl. Phys. **B27**, 598 (1971); T. Kohmura, Prog. Theor. Phys. **46**, 167 (1971); H. Lesniak and L. Lesniak, in Proceedings of the International Conference on High Energy Physics and Nuclear Structure, at Uppsala, Sweden, 1973 (unpublished); Nucl. Phys. **B38**, 221 (1972).

⁸W. R. Gibbs, Phys. Rev. C **3**, 1127 (1971); **5**, 755 (1972); R. Seki, *ibid.* **3**, 454 (1971); L. A. Charleton and J. M. Eisenberg, Ann. Phys. (N.Y.) **63**, 286 (1971).

⁹R. W. Bercaw, J. S. Vincent, E. T. Boschitz, M. Blecher, K. Gotow, D. K. Anderson, R. Kerns, R. Minehart, and K. Ziock, Phys. Rev. Lett. **29**, 1031 (1972).

¹⁰H. H. C. Weidman, M. A. thesis, University of Virginia, 1972 (unpublished).

¹¹B. Zacharov, Nucl. Instrum. Methods **33**, 136 (1965).

¹²C. Lechanoine, M. Martin, and H. Wind, Nucl. Instrum. Methods **69**, 122 (1969).

¹³E. S. Rost, in Lectures from the LAMPF (Clinton P. Anderson Meson Physics Facility) Summer School, on Pion-Nucleus Scattering, July, 1973, edited by W. R. Gibbs and B. F. Gibson, V (Los Alamos Scien-

tific Report No. LA-5443-C, 1973, unpublished), p.135.

¹⁴L. S. Kisslinger, Phys. Rev. 98, 761 (1955).

¹⁵H. R. Collard, L. R. B. Elton, R. Hofstadter, and
H. Schopper, in *Landolt-Börnstein Numerical Data*

and Functional Relationships in Science and Technology,
edited by K. H. Hellwege (Springer-Verlag, Berlin,
1967), New Series, Group 1, Vol. 2.